Visualizing calcium flux in freely moving nematode embryos

Evan L. Ardiel*[1, 2], Abhishek Kumar[1, 2], Joseph Marbach[1], Ryan Christensen[1], Rishi Gupta[1], William Duncan[1], Jonathan S. Daniels[3], Nico Stuurman[4], Daniel Colón-Ramos[5, 6], Hari Shroff[1, 6]

* Correspondence to Evan Ardiel (evan.ardiel@nih.gov)

1. Section on High Resolution Optical Imaging, National Institute of Biomedical Imaging and Bioengineering, National Institutes of Health, Bethesda, Maryland, USA.
2. Grass Lab, Marine Biological Laboratories, Woods Hole, Massachusetts, USA.
3. Applied Scientific Instrumentation, Eugene, Oregon, USA.
4. Howard Hughes Medical Institute & Department of Cellular and Molecular Pharmacology, University of California, San Francisco, California, USA
5. Program in Cellular Neuroscience, Neurodegeneration, and Repair, Department of Cell Biology and Neuroscience, Yale University, New Haven, Connecticut, USA.
6. Whitman Center, Marine Biological Laboratory, Woods Hole, Massachusetts, USA.

Running title: Calcium imaging of *C. elegans* embryos

Abstract

The lack of physiological recordings from *Caenorhabditis elegans* embryos stands in stark contrast to the comprehensive anatomical and gene expression datasets already available. Using light-sheet fluorescence microscopy (LSFM) to address the challenges associated with functional imaging at this developmental stage, we recorded calcium dynamics in muscles and neurons and developed analysis strategies to relate activity and movement. In muscles, we found that the initiation of twitching was associated with a spreading calcium wave in a dorsal muscle bundle. Correlated activity in muscle bundles was linked with early twitching and eventual coordinated movement. To identify neuronal correlates of behavior, we monitored brain-wide activity with subcellular resolution and identified a particularly active cell associated with muscle contractions. Finally, imaging neurons of a well-defined adult motor circuit, we found that reversals in the eggshell correlated with calcium transients in AVA interneurons.

Introduction

Spontaneous neural activity plays an important role in the formation and refinement of developing circuits in many parts of the nervous system. The retina has been a particularly powerful model for studying this phenomena because of its highly organized connections and well-defined cell-types with known physiology[1]. With an invariant cell lineage and reproducible neuronal wiring diagram, the microscopic roundworm, *Caenorhabditis elegans*, offers the opportunity for a systems-level view of spontaneous activity during neurodevelopment. Fourteen hours after fertilization, the 222-cell nervous system of newly hatched larvae supports coordinated movement and even learning[2]. Cell birth times are known[3] and process outgrowths are now being documented[4-7], but functional recordings from muscles or neurons of *C. elegans* embryos have yet to be reported.

Although the nematode's optically and genetically accessible nervous system is ideal for calcium imaging, the embryo's small size, sensitivity to phototoxicity, and rapid movements throughout the 50 x 30 x 30 μm^3 eggshell volume have traditionally complicated image acquisition. We addressed these issues with light-sheet fluorescence microscopy (LSFM), where planar illumination and perpendicular detection enable rapid imaging with efficient optical sectioning and minimal photo-damage[8]. The inverted Selective Plane Illumination Microscope (iSPIM[5,9,10]) implementation is particularly well suited for *C. elegans* embryos because of its high spatial resolution (~0.5 μm laterally, 1.5 μm axially) and compatibility with conventional sample mounting on coverslips. Using open-source control software **(Methods; Fig. S1** in the Supporting Materia**l)** for iSPIM

acquisition, we acquired dozens of images per second for up to 5 Hz volumetric imaging over several minutes across embryogenesis.

After recording unrestrained samples for functional imaging, considerable effort is still required to extract meaning from the raw four-dimensional datasets. The dynamic fluorescence signal must be segmented from the images, tracked in space and time, and mapped back to relevant anatomical and behavioral features. This has only recently been shown to be feasible for large neuronal populations in freely moving adult *C. elegans*[11,12]. The embryo poses unique challenges, as there is more movement in the axial dimension and increased postural diversity compared to a worm crawling on an agar surface. Here we address these analysis challenges to document spreading calcium waves in body wall muscles, record brain-wide activity, and identify neural correlates of behavior during embryogenesis.

Methods

Strains

Animals were maintained on nematode growth medium (NGM) seeded with *Escherichia coli* (OP50). The following strains were imaged: AQ2953 *ljIs131*[*myo-3*p::GCaMP3-SL2-tagRFP-T](GCaMP in body wall muscles)[13], VG563 *unc-13*(*e312*); *ljIs131*(from cross of AQ2953 *ljIs131* and CB312 *unc-13*(*e312*)), ZIM294 *mzmEx199*[*unc-31*p::NLSGCaMP5K; *unc-122*p::GFP](nuclear localized GCaMP expressed panneuronally)[14], and TQ3032 *xuEx1040*[*nmr-1*p::G-CaMP3; *nmr-1*p::DsRed] (GCaMP in AVA interneurons and others)[15].

Light Sheet Microscopy

We used a fiber-coupled diSPIM[16] (Applied Scientific Instrumentation) to perform all imaging experiments. Laser excitation was coupled into a commercially available diSPIM scanhead. The 2D MEMS mirror internal to the scanhead was used to create a light-sheet and in the perpendicular scan direction to define an imaging volume[16]. A lower objective (10x, 0.3 NA, Olympus) was used to find and stage embryos and a pair of perpendicular water-dipping, long-working distance objectives (40x, 0.8 NA, Nikon, Cat. # MRD07420) were used to illuminate the sample and to detect the resulting fluorescence. Although this configuration can be used to collect orthogonal views, here we used a single imaging view for all experiments. A 488 nm long pass filter in the emission arm of the microscope (Semrock, Cat. # LP02-488) was used to eliminate excitation light (~50-300 μW, measured after the objective) before detection on a scientific complementary metal-oxide-semiconductor camera (pco.edge 4.2 or Hamamatsu, ORCA-Flash 4.0).

Micro-Manager

For data acquisition and instrument alignment we used the ASI diSPIM plugin within Micro-manager. Micro-manager is a user-friendly, open-source software platform developed for easy integration of microscopy components and data acquisition[17]. The diSPIM plugin features a graphical user interface for facile control of all diSPIM hardware, including alignment of the light-sheet with the imaging focal plane (via an automated calibration feature) and managing acquisition settings (including laser intensity, number of volumes, number of planes / volume,

inter-volume period, imaging rate; see **Fig. S1**). This open-source plugin has been distributed with Micro-Manager since 2014 and ongoing development continues. Further documentation on the plugin is available at https://micro-manager.org/wiki/ASIdiSPIM_Plugin and http://dispim.org/software/micro-manager.

Imaging Parameters

We acquired iSPIM volumes comprising 30-50 image planes. Exposure time per plane was 2.5-4.5 ms and inter-plane spacing was 1-1.2 um. To maximize speed, embryos were oriented on the cover slip to minimize Z-steps (i.e. embryo long axis perpendicular to optical axis) and the camera was rotated to minimize readout time (i.e. embryo long axis perpendicular to camera chip readout direction), a 90^{o} rotation to that previous reported[5,16]. We imaged embryos at volumetric rates of up to 5 Hz ([2.5 ms exposure/plane + 1.5 ms camera readout] * 30 planes spanning 36 um + 50 ms settle time = 170 ms / volume), but the associated phototoxicity (as determined by delayed hatch time) put an upper limit on the duration of these recordings. Depending on the strain and developmental stage, even 30 min of 2 Hz imaging could delay hatching at the low end of laser powers used here (i.e. 50 μW, measured after the objective).

Sample Preparation

Embryos were obtained from gravid adults, placed on poly-L-lyine coverslips and imaged in M9 buffer as previously described[16]. Prior to light-sheet imaging

139 embryonic stage was determined with brightfield illumination using the lower 10x
140 objective.
141
142 Analysis
143 Body wall muscles:
144 2-fold embryos
145 1) Segmenting muscle quadrants
146 In ImageJ, the Simple Neurite Tracer[18] plugin was used to approximate the
147 position of the body wall muscle quadrants in every third image stack (the same
148 coordinates were used for three consecutive stacks). With Simple Neurite Tracer
149 settings of $\sigma = 2$ and multiplier = 4, the first fold of each muscle bundle could be
150 delineated with 1-3 paths (i.e. 2-4 clicks along the length of the bundle).
151
152 2) Intensity extraction
153 A custom MATLAB script was used to define muscle bundle midlines and
154 extract intensities. Owing to the vertical ('y') orientation of the embryo, we
155 identified the midline at every pixel of the y-dimension. This was done by searching
156 for a local maximum in an xz plane centered on the Simple Neurite Tracer output
157 coordinate and spanning 7 slices in z and 41 pixels in x (i.e. a 7 x 6.7 μm plane).
158 These values are plotted in **Fig. 1c**. To calculate correlation coefficients (with
159 'corrcoef' in MATLAB) between muscle bundles, GCaMP3 intensity was extracted
160 from the bundle cross-sections approximately halfway down the first fold.
161

3) Twitching quantification

In ImageJ, cross-sections were taken at the embryo midpoint and the resulting image was despeckled (3x3 median filter) and smoothed (3x3 mean filter) prior to the use of "Find Maxima..." (with noise tolerance=20) to locate the muscle bundles. The coordinates of local maxima were tracked across frames using u-track 2.0[19], followed by manual confirmation and linking of partial traces.

3-fold embryos

Untwisting software[20] was used to build a 2-dimensional lattice from the position of the GCaMP3-expressing contralateral ventral and dorsal muscle bundles. In the untwisted volumes, bundles were identified and linked across frames, as described for the 2-fold embryo cross-sections (**Fig. 1h**).

Pan-neuronal:

As outlined below, local maxima were identified in each slice and then consolidated in the stack at putative nuclear centers based on position and intensity (**Fig. S4**). The marked nuclear centers were used to facilitate the manual tracking of cells across frames.

1) Local maxima were identified in each slice manually and using the "Find Maxima…" function of ImageJ (noise tolerance=50).
2) A custom MATLAB script linked maxima whose xy positions in adjacent slices were separated by <1.4 μm (i.e. <8 pixels). Nuclear centers were then defined as the intensity peaks through the stack.

3) To facilitate cell tracking, segmented nuclear centers were marked as blue dots on the image. Nuclei were then manually linked across frames in ImageJ. After tracking, errors were identified (and subsequently corrected) by examining:

i) extreme motion, as compared to other nuclei linked over that frame (i.e., if the movement was >4 standard deviations above the mean).

ii) track convergence (i.e., if nuclear separation was <5.6 μm (i.e. <34 pixels)).

iii) inconsistencies between independently derived tracks for the subset of cells with either multiple scorers or multiple attempts from one scorer (i.e., track divergence).

A reviewer manually checked all flagged tracks. Intensity was extracted from a 7 x 7 pixel region centered on the nucleus.

Command interneurons:

Neurons were assigned canonical IDs based on their position relative to other *nmr-1* expressing cells[21]. AVA and AVE cell bodies were not distinguishable due to their close proximity. AVA/AVE, RIM, and PVC cell bodies were manually tracked in maximum intensity projections and cell centers were identified in stacks by examining intensity profiles through the volumes (**Fig. S7**). Following manual confirmation of cell position, intensities were extracted from a 7 x 7 pixel region centered on the cell body. Forward and backward speed was calculated from AVA movement along the vector linking AVA with posteriorly positioned RIM (**Fig. 3a**).

Neural and muscular activity were reported as a fractional intensity change, $dF/F = (F - F_o)/F_o$, where F is the intensity value and F_o is the baseline for an individual muscle bundle, nucleus, or cell body, as defined by its lower 20th percentile intensity value.

Results

Embryonic muscle activity

The 14 h embryogenesis of *C. elegans* consists of two main phases, proliferation and organogenesis. Proliferation ends ~5.5 h post-fertilization at room temperature, at which point the embryo is a spheroid comprising ~550 essentially undifferentiated cells. During organogenesis cells terminally differentiate as the embryo elongates from lima bean shape (~6 h post-fertilization) to two folds (~8 h post-fertization) to three folds (~9 h post-fertilization). Neurite outgrowth coincides with this elongation. Spontaneous muscle contractions ('twitching') begin about 2 h after the transition from proliferation to organogenesis (~8h post-fertilization), at the 1.75-fold stage, before the appearance of neuromuscular junctions[22]. By this point, the body wall muscles have organized into four longitudinal bundles that extend the length of the animal in left and right, dorsal and ventral quadrants. Early spontaneous muscle twitching is essential for viability, as mutants lacking critical muscle genes fail to elongate from ovoid embryo to worm-shaped larva[23]. To characterize the embryo's first twitch we imaged a strain expressing GCaMP3[24] in muscle cells. Embryonic development was monitored with brightfield illumination using the lower 10 x objective. We commenced image

acquisition several minutes before the embryo reached the 1.75-fold stage. Prior to twitching, we observed localized calcium transients that were not associated with muscle contraction **(Movie S1)**. The first twitch was always a discrete event characterized by a large spreading calcium wave and contraction of one of the bundles **(Movie S1)**. In 6 of the 6 embryos tested, the first bundle to contract was dorsally positioned – in 2 embryos it was dorsal left and in 4 embryos it was dorsal right. Some degree of stereotypy in the onset of twitching is perhaps expected, given the invariance of embryogenesis up to this point.

We next investigated activity during early twitching by segmenting and tracking the muscle-localized GCaMP3 intensity. As large contiguous structures, the bundles were fairly easily defined in 1.75 and two-fold embryos with just a few mouse clicks in the Simple Neurite Tracer ImageJ plugin[18] (Methods). Based on the muscle quadrant coordinates so derived, a custom MATLAB script was used to identify midlines, extract intensity, and link bundles across frames. Examining GCaMP3 intensity shortly after the first twitch, in two-fold embryos, we counted multiple calcium waves per minute in all quadrants **(Fig 1a-c; Fig. S2; Movie S2)**. In addition to waves, we also observed bursts of fluorescence intensity that were localized within each bundle in both the first and second folds **(Fig. S2)**. Calcium transients were associated with muscle contraction, as revealed by a shortening of the bundle **(Fig. 1c)**. We were able to link calcium transients to the motion of the animal using axial rotation as a quantitative behavioral metric **(Fig. 1d)**: the muscle bundles were automatically identified as local maxima from a cross-section at the midpoint and u-track 2.0[19] with manual editing was used to link them across frames

(Methods). Instances of accelerated angular velocity were associated with correlated events in left and right dorsal or ventral bundles **(Fig. 1e)**.

To further investigate the developmental time course of early contractions, we staged six 1.75-fold embryos and imaged 3 min 20 s of muscle activity within 10 min of the first twitch and then again 20 min later. GCaMP3 intensity was extracted from the bundle cross-sections approximately halfway down the first fold. Post-embryonically, left and right muscle bundle pairs are electrically coupled, but ipsilateral dorsal and ventral bundles are not[25]. To test for bundle coupling, we calculated the correlation coefficient of fluorescence intensity between bundles. Strong positive correlations were observed between left-right pairs, particularly at the second time point (**Fig. 1f**), suggesting the formation of inter-bundle junctions during the transition from 1.75 to 2-fold stage. Consistent with a lack of electrical coupling, no significant positive correlations were observed in ipsilateral dorsal or ventral bundles (**Fig. 1f**). Although negative correlations between these bundles is reminiscent of the alternating dorso-ventral muscle contractions underlying sinusoidal locomotion postembryonically[13,26], the requisite neuromuscular junctions are not apparent in EM at this stage of embryogenesis[22]. Consistent with the hypothesis that the earliest twitches are myogenic and not controlled by the nervous system, perturbing synaptic release with a mutant allele of *unc-13*[27] did not impair the emergence of correlated activity in left-right muscle bundles (**Fig. 1f**). Furthermore, despite severe locomotion deficits post-hatching[28], movement of *unc-13* mutant embryos was statistically indistinguishable from controls at the 1.75/two-fold stage (**Fig. 1g**).

Twitching is initially driven by spontaneous muscle contractions, but hours after the first twitch, during the three-fold stage, neuromuscular junctions appear and movement becomes more coordinated, suggesting some degree of motor control[22]. To visualize muscle dynamics in three-fold embryos, we imaged at rates up to 5 Hz (volumetric; **Movie S3**). Detailed examination of these dynamics is confounded by the convoluted embryo posture. To map calcium traces onto a common coordinate system, we adapted recently-developed software for computationally straightening three-fold embryos[6] . Although designed for a specific set of markers, body wall muscle fluorescence provided sufficient structure for the software to define a worm shape and untwist it. After untwisting, GCaMP intensity could be extracted from any position along the muscle bundle **(Fig. 1h-i; Movie S4)**. The ability to track muscle activity throughout embryogenesis provides a window into neurodevelopment, as spontaneous contractions shift to coordinated motor output presumably mediated by the nervous system.

Brain-wide calcium imaging at subcellular resolution in a freely behaving embryo

We next attempted to characterize calcium flux in neurons directly. Recent technological advances in microscopy, combined with better fluorescent probes, have enabled near-brain-wide calcium imaging in immobilized worms, flies, and flies, and fish[14,29,30]. This was even recently demonstrated in freely behaving embryonic *Drosophila*[31] and adult *C. elegans* [11,12]. Despite the challenges associated with imaging a compact and entangled nervous system with significant movement

in the axial dimension, the *C. elegans* embryo offers certain advantages for pan-neuronal imaging; it has fewer neurons than the adult (222 in the embryo versus 302 in the adult hermaphrodite) and its behavior is naturally confined within the eggshell – nature's own microfluidic device. To evaluate global brain dynamics with subcellular resolution in a freely behaving *C. elegans* embryo, we used a strain expressing nuclear-localized GCaMP5K[32] from a pan-neuronal promoter[14]. Nuclear localization is essential for segmenting cells in the densely populated ganglia. Nuclear GCaMP will not report activity compartmentalized in neurites[33], but the large calcium permeable nucleus is at least a good proxy for the cell body[14], where most postembryonic calcium imaging studies have been performed.

We recorded two 3.5 min sessions of activity in the early and mid three-fold stages, at a 1.4 Hz volumetric rate. To facilitate manual linking across frames, we first labeled nuclei centers based on the position and intensity of local maxima in each slice **(Methods)**. We tracked 65 cells across all frames of imaging session 1 **(Fig. 2a; Fig. S3; Fig. S4; Movie S5)**. From this dataset, one cell (termed "cell 1" in **Figure 2**) stood out as particularly active, with multiple large intensity spikes **(Fig. 2b)**. Its high level of activity relative to the nearest ventral nerve cord (VNC) motor neurons (positioned along the longitudinal axis of the embryo, i.e. cells 44, 3, 26, and 6) was readily apparent **(Fig. 2c)** and suggests that imaging **(Fig. S5)** or motion artifacts cannot explain the observed intensity fluctuations. We also found that the intensity fluctuations observed in cell 1 were associated with a shortening of the vector connecting the VNC nuclei anterior and posterior to the active cell **(Fig. 2b-c)**. VNC motor neurons have been shown to have proprioceptive properties[34], but

323 further work is needed to determine if this cell is eliciting and/or detecting the
324 associated muscle contractions. The relative inactivity of other cells may arise from
325 the incomplete representation of neural activity at the cell body at this
326 developmental stage.
327 Canonical cell identities were not known, but positional information could be
328 used to identify the same cells in multiple imaging sessions across embryogenesis.
329 Indeed, although increased movement with development made tracking more
330 difficult **(Movie S6; Fig. S6)**, we were able to follow many of the same cells two
331 hours later, including the particularly active cell described above. Again we
332 observed that a shortening of the vector connecting its anterior and posterior nuclei
333 correlated with calcium events that were larger and more frequent than in
334 neighboring cells **(Fig. 2d)**. Although we could not assign a canonical ID to this
335 particularly active cell, we did search other embryos for similarly positioned nuclei
336 with calcium transients correlated with local muscle contractions. We identified one
337 such candidate from five recordings of early three-fold embryos **(Fig. S6)**.
338 Monitoring large populations of neurons, at single-cell resolution, in freely behaving
339 animals is essential for understanding nervous system control of motor output, yet--
340 perhaps due to technical difficulties associated with image acquisition and analysis--
341 such efforts remain scarce. Future work is aimed at strategies to unambiguously
342 identify neurons within these large ensembles (an unsolved problem in general), to
343 enable comparisons among animals and modeling of behavior at the cellular scale[35].
344
345 **Reversals in the eggshell are associated with AVA activity**

Using sparser labels it is possible to track embryonic calcium activity in groups of cells whose identities are known. Cell ablation, calcium imaging, and optogenetic activation experiments have implicated bilaterally symmetrical AVA as the command interneurons driving reversals in larvae and adults[36-38]. To determine if a similar circuit mediated reversals of the embryo, we tracked calcium dynamics in AVA using a strain driving GCaMP3 from the *nmr-1* promoter, which expresses in 6 neuron classes, including AVA[21]. In late stage three-fold embryos, calcium events were apparent in cell bodies and processes in the nerve ring and ventral nerve cord **(Movie S7)**. Measuring the mean intensity of the entire frame, we observed large fluctuations (dF/F>0.6) in 6 of 17 embryos (**Fig. S7**). To identify the source of the signal and describe embryonic movement, we manually tracked AVA, RIM, and PVC cell bodies in three of these recordings. Movement along the vector linking AVA and RIM was used to calculate the velocity of the head along the longitudinal axis of the worm (**Fig. 3a**). In 2 of the 3 embryos analyzed, there was a significant negative correlation between instantaneous velocity and mean intensity of that frame (**Fig. 3b**). This significant negative correlation was also apparent using intensity derived from either of the AVA cell bodies (**Fig. 3b**). However, there was no significant relationship between velocity and intensity derived from a PVC cell body (PVC is a class of interneurons in the tail contributing to stimulated forward movement in adults[36,39]). Examining the traces, it is clear that the temporal coupling of backward movement and AVA activity in embryos is not as tight as in hatched animals crawling on agar[37,40,41]. This could be the result of the immature state of the motor circuit or movement constraints imposed by the eggshell. Nonetheless, at some

point before hatching, the *C. elegans* embryo is capable of coordinated behaviors associated with similar circuitry as in the adult.

Discussion

iSPIM allowed us to interrogate calcium flux in freely behaving *C. elegans* embryos with negligible phototoxicity, at subsecond temporal resolution, and submicron spatial resolution. With these capabilities we linked muscle and neural activity with movement. In order to study embryos with diverse GCaMP localization, we developed several custom semi-automated analysis pipelines that facilitated segmentation and tracking of dynamic changes in fluorescence intensity and subsequent correlation with behavioral metrics (rotation, movement) that were also derived from the underlying image data. We discovered that twitching initiates in dorsal muscle bundles and we documented the early correlated activity that drives axial rotation. We recorded brain-wide calcium dynamics and showed that reversals in the eggshell are associated with activity of the reversal command interneurons, AVAL and AVAR.

Anticipated improvements in instrumentation to enable better optical sectioning[42], higher resolution, increased collection efficiency, and faster acquisition will further facilitate automation of cell segmentation and tracking over longer time periods. Documenting early muscle dynamics and twitches will lead to a better understanding of elongation, while examining the transition to coordinated movement will lead to insights into motor system development. In neurons, functional data will help to define the relationship between activity, process

outgrowth, and synaptogenesis. While adult locomotion has been the focus of much research[43-45], movement of the embryo remains almost completely unexplored. Detailed behavioral characterization of the embryo in the post-twitching regime will help focus future calcium imaging experiments to periods when neural circuits are wiring up and coming online. We anticipate that functional data will add a valuable layer of information to cross-reference with the rich anatomical and gene expression datasets already available in *C. elegans*[46].

Author Contributions

E.A. and A.K. conceived the project. E.A., A.K., and H.S. designed experiments. E.A. and A.K. acquired data. E.A., J.M., R.C., R.G., W.D., and H.S. analyzed data. A.K. built the system. J.D. and N.S. wrote the u-manager diSPIM plugin and tested it with assistance from A.K. E.A. and H.S. wrote the paper with input from all authors. D.C-R. and H.S. supervised the research.

Acknowledgements.

Strains were provided by Manuel Zimmer and the CGC (funded by NIH Office of Research Infrastructure Programs P40 OD010440). We thank Applied Scientific Instrumentation (ASI) for lending us a diSPIM frame, Mark Reinhardt and PCO for lending us scientific CMOS cameras, and Lynne Chang and Nikon for lending us objectives. We thank K. Joy, L. Joy, N. Kattapuram, and Y. Oyhama for help with manual tracking, V. Periwal (NIDDK), J. Hawk (Yale University), and H. Vishwasrao (NIH) for useful discussions regarding calcium imaging, and M. Kittelberger and K. Khodakhah for guidance and leadership in the Grass Lab. E.A. and A.K. acknowledge support from the Grass Fellowship Program and D. C-R. and H.S. acknowledge the Whitman Fellowship program at MBL. Some data were collected as part of the MBL Neurobiology course with the assistance of T. Graham and A. Thompson. We also thank the Research Center for Minority Institutions program and the Institute of Neurobiology at the University of Puerto Rico for providing a meeting and brainstorming platform. This work was supported by the intramural research program of the National Institute of Biomedical Imaging and Bioengineering and NIH grants U01 HD075602 and R24OD016474 to D.C-R and A.K.

Disclaimer: The NIH, its employees, and officers do not recommend or endorse any company, product, or service.

Figure 1. **High speed interrogation of muscular calcium dynamics in the post-twitching embryo. a)** Two-fold embryo expressing GCaMP3 from a *myo-3* promoter, as seen in lateral maximum intensity projection (top) and cross section through the volume at dotted white line (bottom). Quadrants are colored identically in **a, c, d**. See also **Movie S2**. **b)** Representative projections (top) and cross sections (bottom) at indicated time points, emphasizing spreading calcium waves (top, magenta) and rotation of animal (bottom). Dotted ellipses in bottom row encircle left and right muscle bundles. **c)** Fluorescence intensity along each bundle over time. Dashed lines in **c, e** denote time window highlighted in **b**. **d)** Angular coordinate system from which rotation behavior is quantified in **e**. **f)** Correlation coefficients for fluorescence intensity in left-right and ipsilateral muscle bundle pairs. Each row corresponds to an embryo in one of two imaging sessions (time 1 or time 2). Imaging sessions were 3 min 20 s in duration and separated by 20 minutes during the 1.75 to 2-fold transition. **g)** Minimum to maximum angular change/minute during time window 1 and 2. Open circles indicate measurements derived from individual embryos and black crosses correspond to mean +/- SEM. Asterisks and 'n.s.' denote statistically distinguishable (paired *t*-test, $p < 0.05$) and indistinguishable (unpaired *t*-test, $p < 0.05$) groups, respectively. **h)** Representative maximum intensity projections (left) and cross sections (right) at select time points in the untwisted reference frame. See also **Movie S4**. **i)** Fluorescence traces for each bundle at location indicated by dotted white line in **h** (scale bars: 5s (horizontal) and dF/F=2 (vertical)). All other scale bars: 10μm (horizontal). Inset: Dotted ellipses encircle left and right muscle bundles in the cross-section. Volumetric imaging was

performed at 2Hz for **b-e** and **h-i** and 1Hz for **f-g**. The ImageJ Fire LUT was used in **b** and **h**.

Figure 2. Brain-wide neuronal imaging in the 3-fold embryo. **a)** dF/F traces for neuronal nuclei tracked from an early 3-fold embryo expressing nuclear localized GCaMP5K from an *unc-31* promoter. Cells are sorted by degree of correlation with the most active cell (i.e., neuron #1 in **a-d**). **b)** Representative maximum intensity projections (left; coel=GFP expressing coelomocytes) and corresponding schematic representations (right; color and size of nuclei correspond to dF/F). Scale bar: 10μm (horizontal). See also **Movie S5**. **c)** 1/length indicated in **b** and dF/F traces for specified neuronal nuclei. Note the correlation between length metric (black) and activity of neuron #1. Grey band denotes time window highlighted in **b**. **d)** Time point 2, 2h after **c**. Imaging was performed at 1.4Hz (volumetric).

Figure 3. Linking behavior to calcium activity in command interneurons. **a)** Left: Maximum intensity projections of a late 3-fold embryo expressing GCaMP3 from an *nmr-1* promoter. Velocity was calculated along the vector linking AVA and RIM. Scale bar: 10 μm (horizontal). The ImageJ Fire look up table was used for display. See also **Movie S7. b)** Velocity and mean fluorescence intensity of entire frame (above). Fluorescence intensity traces of tracked AVAL, AVAR, and PVC cell bodies from two embryos (left and right). Vertical dashed lines highlight the period depicted in **a**. Imaging was performed at 1.4 Hz (volumetric). Correlation coefficients for velocity and intensity are indicated on figure.

References

1 Blankenship, A. G. & Feller, M. B. Mechanisms underlying spontaneous patterned activity in developing neural circuits. *Nat Rev Neurosci.* **11**, 18-29 (2010).

2 Jin, X., Pokala, N. & Bargmann, C. I. Distinct Circuits for the Formation and Retrieval of an Imprinted Olfactory Memory. *Cell* **164**, 632-643. (2016).

3 Sulston, J. E., Schierenberg, E., White, J. G. & Thomson, J. N. The embryonic cell lineage of the nematode Caenorhabditis elegans. *Dev. Biol.* **100**, 64-119 (1983).

4 Heiman, M. & Shaham, S. DEX-1 and DYF-7 establish sensory dendrite length by anchoring dendritic tips during cell migration. *Cell* **137**, 344-355 (2009).

5 Wu, Y. *et al.* Inverted selective plane illumination microscopy (iSPIM) enables coupled cell identity lineaging and neurodevelopmental imaging in Caenorhabditis elegans. *Proc. Natl. Acad. Sci. USA* **108**, 17708-17713 (2011).

6 Christensen, R. *et al.* Untwisting the Caenorhabditis elegans embryo. *eLife*, e10070 (2015).

7 Singhal, A. & Shaham, S. Infrared laser-induced gene expression for tracking development and function of single C. elegans embryonic neurons. *Nat Commun.* **8**, 14100 (2017).

8 Keller, P. J., Ahrens, M. B. & Freeman, J. Light-sheet imaging for systems neuroscience. *Nature Methods* **12**, 27-29 (2015).

9 Wu, Y. *et al.* Spatially isotropic four-dimensional imaging with dual-view plane illumination microscopy. *Nat Biotechnol.* **31**, 1032-1038 (2013).

10 Kumar, A., Colon-Ramos, D. & Shroff, H. Watching a roundworm develop with a sheet of light. *Physics Today* **68**, 58-59 (2015).

11 Nguyen, J. P. *et al.* Whole-brain calcium imaging with cellular resolution in freely behaving Caenorhabditis elegans. . *Proc Natl Acad Sci U S A* **113**, E1074-1081 (2016).

12 Venkatachalam, V. *et al.* Pan-neuronal imaging in roaming Caenorhabditis elegans. *Proc Natl Acad Sci U S A* **113**, E1082-1088 (2016).

13 Butler, V. J. *et al.* A consistent muscle activation strategy underlies crawling and swimming in Caenorhabditis elegans. . (2015).

14 Schrodel, T., Prevedal, R., Aumayr, K., Zimmer, M. & Vaziri, A. Brain-wide 3D imaging of neuronal activity in Caenorhabditis elegans with sculpted light. *Nature Methods* **10**, 1013-1020 (2013).

15 BJ, P., J, L., Z, F., SA, W. & XZ., X. The neural circuits and synaptic mechanisms underlying motor initiation in C. elegan. *Cell* **147**, 922-933 (2011).

16 Kumar, A. *et al.* Dual-view plane illumination microscopy for rapid and spatially isotropic imaging. *Nature Protocols* **9**, 2555-2573 (2014).

17 Edelstein AD, T. M., Amodaj N, Pinkard H, Vale RD, Stuurman N. Advanced methods of microscope control using μManager software. *J Biol Methods.* **1**, e10 (2014).

18 Longair, M. H., Baker, D. A. & Armstrong, J. D. Simple Neurite Tracer: open source software for reconstruction, visualization, and analysis of neuronal processes. *Bioinformatics* **27**, 2453-2454 (2011).

19 Jaqaman, K. *et al.* Robust single-particle tracking in live-cell time-lapse sequences. *Nat Methods* **5**, 695-702 (2008).
20 Christensen, R. *et al.* An imaging and analysis toolset for the study of Caenorhabditis elegans neurodevelopment. *SPIE BiOS*, 93340C-93340C-93349 (2015).
21 Brockie, P. J., Mellem, J. E., Hills, T., Madsen, D. M. & A.V., M. The C. elegans glutamate receptor subunit NMR-1 is required for slow NMDA-activated currents that regulate reversal frequency during locomotion. . *Neuron* **31**, 617-630 (2001).
22 Durbin, R. M. Studies on the Development and Organization of the Nervous System of Caenorhabditis elegans. *Thesis* (1987).
23 Williams, B. D. & Waterston, R. H. Genes critical for muscle development and function in Caenorhabditis elegans identified through lethal mutations. *J Cell Biol.* **124**, 475-490 (1994).
24 Tian, L. *et al.* Imaging neural activity in worms, flies, and mice with improved GCaMP calcium indicators. *Nature Methods* **6**, 875-881 (2009).
25 Liu, Q., Chen, B., Gaier, E., Joshi, J. & Wang, Z. W. Low conductance gap junctions mediate specific electrical coupling in body-wall muscle cells of Caenorhabditis elegans. *J Biol Chem.* **281**, 7881-7889 (2006).
26 Zhen M, S. A. C. elegans locomotion: small circuits, complex functions. *Curr Opin Neurobiol* **33**, 117-126 (2015).
27 Richmond, J. E., Davis, W. S. & Jorgensen, E. M. UNC-13 is required for synaptic vesicle fusion in C. elegans. . *Nat Neurosci.* **2**, 959-964 (1999).
28 Brenner, S. The genetics of Caenorhabditis elegans. *Genetics* **77**, 71-94 (1974).
29 Lemon, W. C. *et al.* Whole-central nervous system functional imaging in larval Drosophila. . *Nat Commun.* **6**, 7924 (2015).
30 Ahrens, M. B., Orger, M. B., Robson, D. N., Li, J. M. & Keller, P. J. Whole-brain functional imaging at cellular resolution using light-sheet microscopy. *Nat Methods* **10**, 413-420 (2013).
31 Chhetri, R. K. *et al.* Whole-animal functional and developmental imaging with isotropic spatial resolution. *Nature Methods* **12**, 1171-1178 (2015).
32 Akerboom, J. *et al.* Optimization of a GCaMP calcium indicator for neural activity imaging. *J Neurosci.* **32**, 13819-13840 (2012).
33 Hendricks, M., Ha, H., Maffey, N. & Zhang, Y. Compartmentalized calcium dynamics in a C. elegans interneuron encode head movement. *Nature* **487**, 99-103 (2012).
34 Wen, Q. *et al.* Proprioceptive coupling within motor neurons drives C. elegans forward locomotion. . *Neuron* **76**, 750-761 (2012).
35 Kato S, K. H., Schrödel T, Skora S, Lindsay TH, Yemini E, Lockery S, Zimmer M. Global brain dynamics embed the motor command sequence of Caenorhabditis elegans. *Cell* **163(3):656-69**, 656-669 (2015).
36 Chalfie, M. *et al.* The neural circuit for touch sensitivity in Caenorhabditis elegans. . *J Neurosci.* **5**, 956-964. (1985).

37 Chronis, N., Zimmer, M. & Bargmann, C. I. Microfluidics for in vivo imaging of neuronal and behavioral activity in Caenorhabditis elegans. . *Nat Methods* **4**, 727-731 (2007).
38 Schmitt, C. *et al.* Specific expression of channelrhodopsin-2 in single neurons of Caenorhabditis elegans. . *PLoS One* **7**, e43164 (2012).
39 Wicks, S. R., Roehrig, C. J. & Rankin, C. H. A dynamic network simulation of the nematode tap withdrawal circuit: predictions concerning synaptic function using behavioral criteria. . *J Neurosci.* **16**, 4017-4031 (1996).
40 Kawano, T. *et al.* An imbalancing act: gap junctions reduce the backward motor circuit activity to bias C. elegans for forward locomotion. . *Neuron* **72**, 572-586 (2011).
41 Ben Arous, J., Tanizawa, Y., Rabinowitch, I., Chatenay, D. & Schafer, W. R. Automated imaging of neuronal activity in freely behaving Caenorhabditis elegans. . *J. Neurosci Methods* **187**, 229-234 (2010).
42 Kumar, A. *et al.* Using stage- and slit-scanning to improve contrast and optical sectioning in dual-view inverted light-sheet microscopy (diSPIM). *The Biological Bulletin* **231**, 26-39 (2016).
43 Stephens, G. J., Johnson-Kerner, B., Bialek, W. & Ryu, W. S. Dimensionality and dynamics in the behavior of C. elegans. *PLoS Comput Biol.* **4**, e1000028 (2008).
44 Yemini, E., Jucikas, T., Grundy, L. J., Brown, A. E. & Schafer, W. R. A database of Caenorhabditis elegans behavioral phenotypes. *Nat Methods* **10**, 877-879 (2013).
45 Schwarz, R. F., Branicky, R., Grundy, L. J., Schafer, W. R. & Brown, A. E. Changes in Postural Syntax Characterize Sensory Modulation and Natural Variation of C. elegans Locomotion. *PLoS Comput Biol.* **11**, e1004322 (2015).
46 Santella, A. *et al.* WormGUIDES: an interactive single cell developmental atlas and tool for collaborative multidimensional data exploration. . *BMC Bioinformatics* **16**, 1-9 (2015).

Fig 1

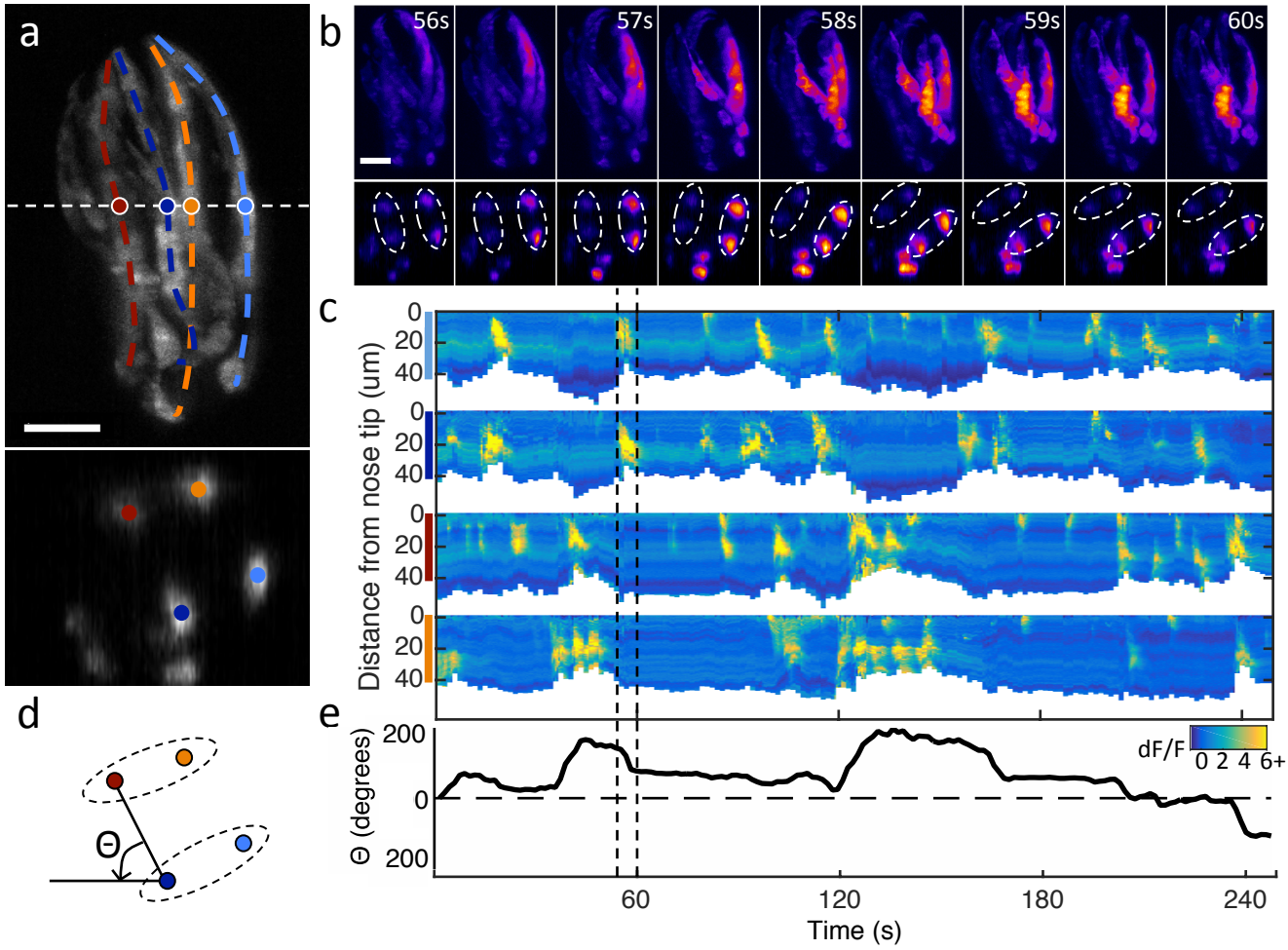
a
b
56s
57s
58s
59s
60s
c
Distance from nose tip (um)
0
20
40
d
Θ
e
Θ (degrees)
200
0
200
dF/F
0 2 4 6+
60
120
180
240
Time (s)
f
embryo
L-R
L-L & R-R
L-R
L-L & R-R
time 1
time 2
1
2
3
4
5
6
R
1
0
-1
control
unc-13
g
Rotations (degrees/min)
300
200
100
0
n.s.
*
*
1
2
1
2
control
unc-13
h
20s
26s
32s
i
1
2

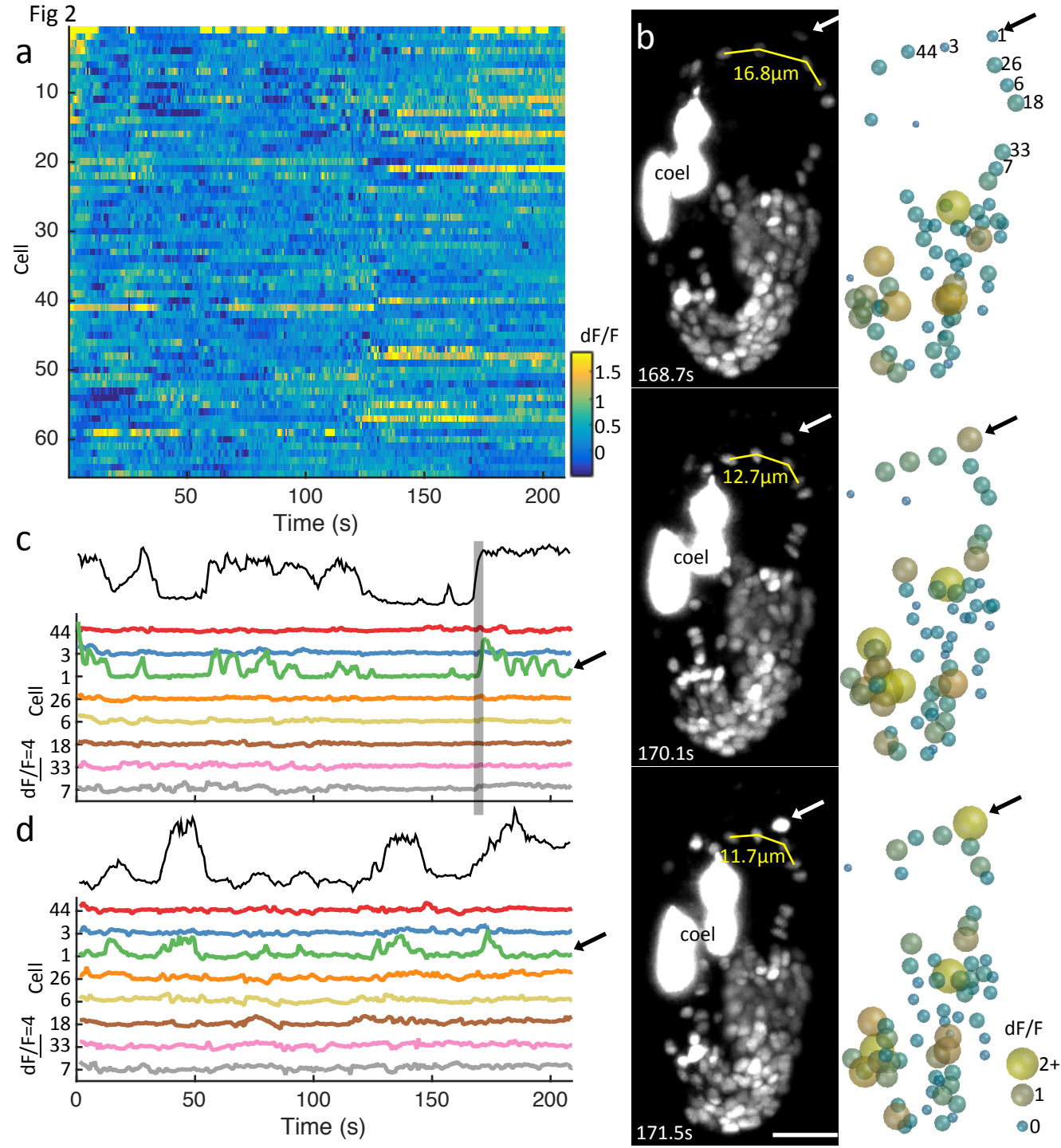
Fig 2
a
Cell
10
20
30
40
50
60
50
100
150
200
Time (s)
dF/F
1.5
1
0.5
0
b
16.8µm
coel
168.7s
12.7µm
coel
170.1s
11.7µm
coel
171.5s
1
44
3
26
6
18
33
7
dF/F
2+
1
0
c
Cell
dF/F=4
44
3
1
26
6
18
33
7
d
Cell
dF/F=4
44
3
1
26
6
18
33
7
0
50
100
150
200
Time (s)

Fig 3

a

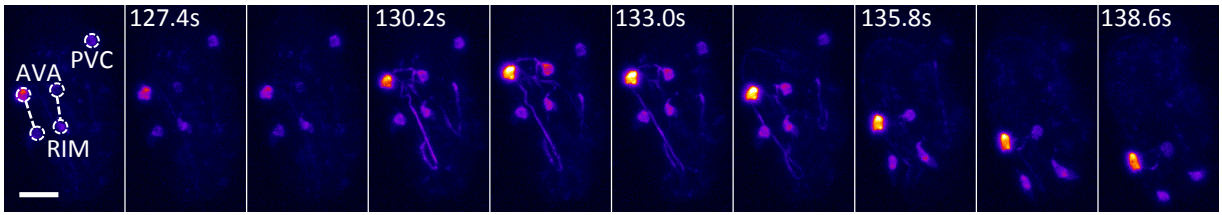
AVA
PVC
RIM
127.4s
130.2s
133.0s
135.8s
138.6s

b

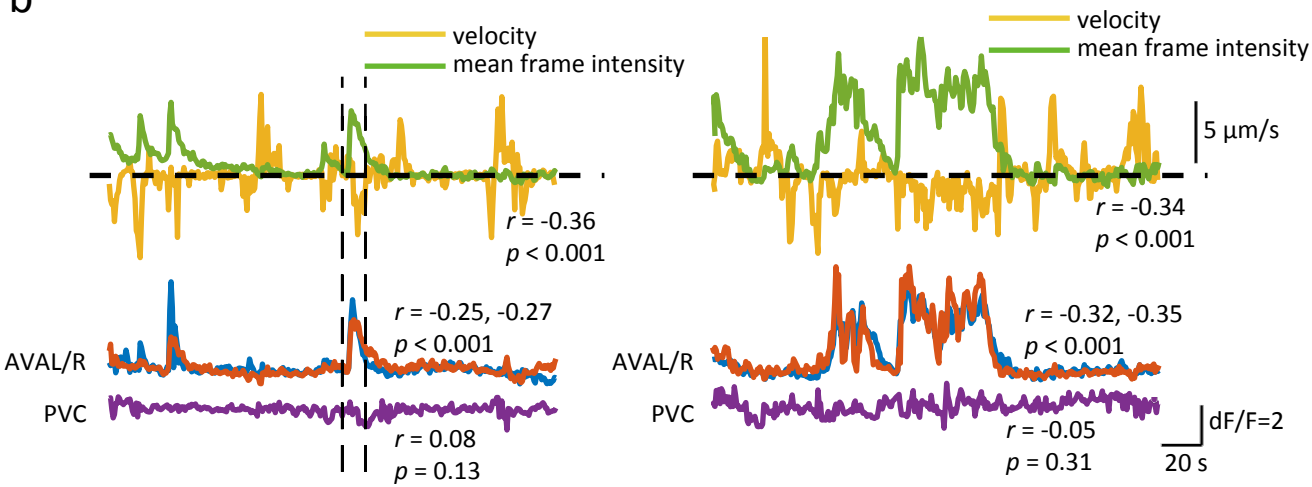
velocity
mean frame intensity
r = -0.36
p < 0.001
AVAL/R
r = -0.25, -0.27
p < 0.001
PVC
r = 0.08
p = 0.13
velocity
mean frame intensity
5 µm/s
r = -0.34
p < 0.001
AVAL/R
r = -0.32, -0.35
p < 0.001
PVC
r = -0.05
p = 0.31
dF/F=2
20 s

Supporting Material

Visualizing calcium flux in freely moving nematode embryos

Evan Ardiel*[1, 2], Abhishek Kumar[1, 2], Joseph Marbach[1], Ryan Christensen[1], Rishi Gupta[1], William Duncan[1], Jonathan S. Daniels[3], Nico Stuurman[4], Daniel Colón-Ramos[5, 6], Hari Shroff[1, 6]

* Correspondence to Evan Ardiel (evan.ardiel@nih.gov)

1. Section on High Resolution Optical Imaging, National Institute of Biomedical Imaging and Bioengineering, National Institutes of Health, Bethesda, Maryland, USA.
2. Grass Lab, Marine Biological Laboratories, Woods Hole, Massachusetts, USA.
3. Applied Scientific Instrumentation, Eugene, Oregon, USA.
4. Howard Hughes Medical Institute & Department of Cellular and Molecular Pharmacology, University of California, San Francisco, California, USA
5. Program in Cellular Neuroscience, Neurodegeneration, and Repair, Department of Cell Biology and Neuroscience, Yale University, New Haven, Connecticut, USA.
6. Whitman Center, Marine Biological Laboratory, Woods Hole, Massachusetts, USA.

Figure S1. Micro-manager plugin. Screenshots of the setup **(a)** and acquisition tabs **(b)**. Further documentation on the plugin is available at https://micro-manager.org/wiki/ASIdiSPIM_Plugin and http://dispim.org/software/micro-manager.

Figure S2. Calcium events in muscles of two-fold embryos. Raster plots duplicated from **Fig. 1c** with traces of mean dF/F of the bundle. Open circles denote calcium waves (peaks separated by at least 5 s with dF/F > 1.5), while arrows denote more localized events. Imaging was performed at 2 Hz (volumetric).

Figure S3. Cell counts. Number of *unc-31* expressing cells at various stages of embryogenesis. The 2-fold cell counts are from three different embryos, while the 3-fold cell counts are derived from the embryo described in text. Circles correspond to individual volume counts.

Figure S4. Segmenting nuclei. 5 of 40 slices raw **(a)** or with colored dots denoting local maxima **(b)** or nuclear centers **(c)**. Scale bar: 10μm.

Figure S5. Fluorescein fluorescence control. To ensure that intensity changes in excitation did not cause significant fluctuations in GCaMP, we measured the apparent intensity of a uniform fluorescein dye solution under conditions identical to those in the experiments in **Fig. 2**. **a)** Representative maximum projection

showing the positions at which fluorescein intensity was measured over time. **b)** dF/F traces across 298 frames (positions indicated in **a**).

Figure S6. Pan-neuronal imaging. a) dF/F traces for neuronal nuclei tracked from a mid-3-fold (2 hours after the dataset presented in **Fig. 2**) embryo expressing nuclear-localized GCaMP5K from an *unc-31* promoter. Cell 1 here matches cell 1 in **Fig 2**. **b)** 1/length (as indicated in **Fig. 2b**) and dF/F traces for ventral nerve cord neurons. Note the correlation between the length metric (black) and the top trace. Imaging was performed at 1.4 Hz (volumetric).

Figure S7. Determining measurement regions in AVA datasets. a) Maximum intensity projections of an embryo expressing GCaMP3 from an *nmr-1* promoter. Scale bar: 10μm. **b)** Intensity profile through the stack at crosses shown on left. Peak location defines the slice from which intensity is extracted for each cell. **c)** Whole image dF/F traces for 17 embryos. Arrowheads indicate traces with dF/F events > 0.6 and double arrowheads indicate samples in which cell bodies were tracked. Imaging was performed at 1.4 Hz (volumetric).

Movie S1. Lateral maximum intensity projection of 4 embryos at the 1.75-fold stage expressing GCaMP3 in muscle cells. Panels are synchronized to first twitch (at t=100s). Scale bar: 10μm. Imaging was performed at 2 Hz (volumetric).

Movie S2. Two-fold embryo expressing GCaMP3 in muscle cells. Lateral maximum intensity projection (top) and cross-sectional view (bottom, corresponding to white line in top panel). Scale bar: 10μm. Imaging was performed at 2 Hz (volumetric).

Movie S3. Lateral maximum intensity projection of a three-fold embryo expressing GCaMP3 in muscle cells. Scale bar: 10μm. Imaging was performed at 5 Hz (volumetric).

Movie S4. Three-fold embryo expressing GCaMP3 in muscle cells. Maximum intensity projections before (left) and after (middle) computational untwisting. Yellow line denotes the position of the cross-section shown at upper right. Scale bar: 10μm. Imaging was performed at 2 Hz (volumetric).

Movie S5. Early three-fold embryo expressing nuclear localized GCaMP5K from an *unc-31* promoter. Lateral maximum intensity projection (left) and corresponding schematic representations of dF/F (right; color and size scale corresponds to dF/F= 0, 1, and 2+). Scale bar: 10μm. Imaging was performed at 1.4 Hz (volumetric).

Movie S6. Mid-stage three-fold embryo expressing nuclear localized GCaMP5K from an *unc-31* promoter. Lateral maximum intensity projection (left) and corresponding schematic representations of dF/F (right; color and size scale corresponds to dF/F= 0, 1, and 2+). Scale bar: 10μm. 1.4 Hz (volumetric).

Movie S7. Maximum intensity projection of a late three-fold embryo expressing GCaMP3 from an *nmr-1* promoter (ImageJ Fire look up table was used for display). Scale bar: 10μm. 1.4 Hz (volumetric).

Supp Fig 1

a

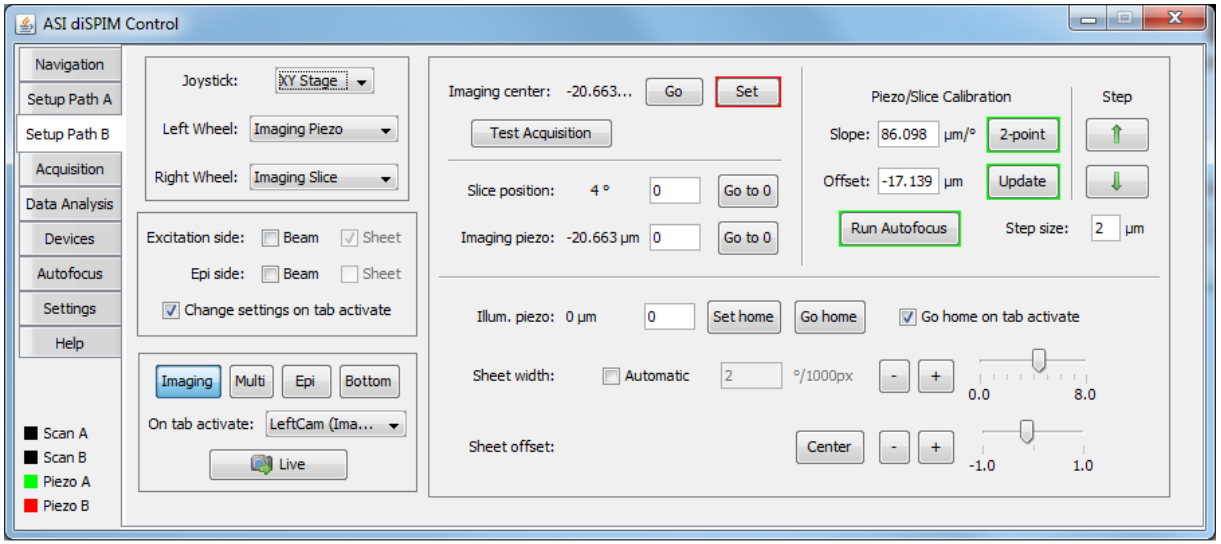
ASI diSPIM Control
Navigation
Setup Path A
Setup Path B
Acquisition
Data Analysis
Devices
Autofocus
Settings
Help
Scan A
Scan B
Piezo A
Piezo B
Joystick: XY Stage
Left Wheel: Imaging Piezo
Right Wheel: Imaging Slice
Excitation side: Beam Sheet
Epi side: Beam Sheet
Change settings on tab activate
Imaging Multi Epi Bottom
On tab activate: LeftCam (Ima...
Live
Imaging center: -20.663... Go Set
Test Acquisition
Slice position: 4 ° 0 Go to 0
Imaging piezo: -20.663 µm 0 Go to 0
Piezo/Slice Calibration
Slope: 86.098 µm/° 2-point
Offset: -17.139 µm Update
Run Autofocus
Step
Step size: 2 µm
Illum. piezo: 0 µm 0 Set home Go home
Go home on tab activate
Sheet width: Automatic 2 °/1000px
0.0 8.0
Sheet offset: Center
-1.0 1.0

b

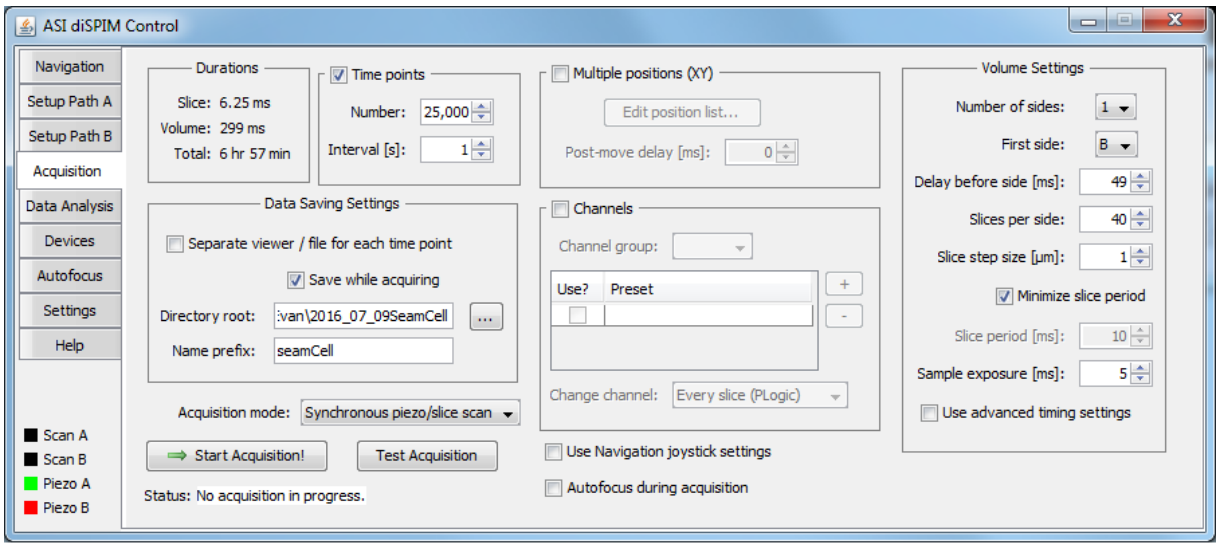
ASI diSPIM Control
Navigation
Setup Path A
Setup Path B
Acquisition
Data Analysis
Devices
Autofocus
Settings
Help
Scan A
Scan B
Piezo A
Piezo B
Durations
Slice: 6.25 ms
Volume: 299 ms
Total: 6 hr 57 min
Time points
Number: 25,000
Interval [s]: 1
Multiple positions (XY)
Edit position list...
Post-move delay [ms]: 0
Volume Settings
Number of sides: 1
First side: B
Delay before side [ms]: 49
Slices per side: 40
Slice step size [µm]: 1
Minimize slice period
Slice period [ms]: 10
Sample exposure [ms]: 5
Use advanced timing settings
Data Saving Settings
Separate viewer / file for each time point
Save while acquiring
Directory root: :van\2016_07_09SeamCell
Name prefix: seamCell
Channels
Channel group:
Use? Preset
Change channel: Every slice (PLogic)
Acquisition mode: Synchronous piezo/slice scan
Start Acquisition!
Test Acquisition
Use Navigation joystick settings
Autofocus during acquisition
Status: No acquisition in progress.

Supp Fig 2

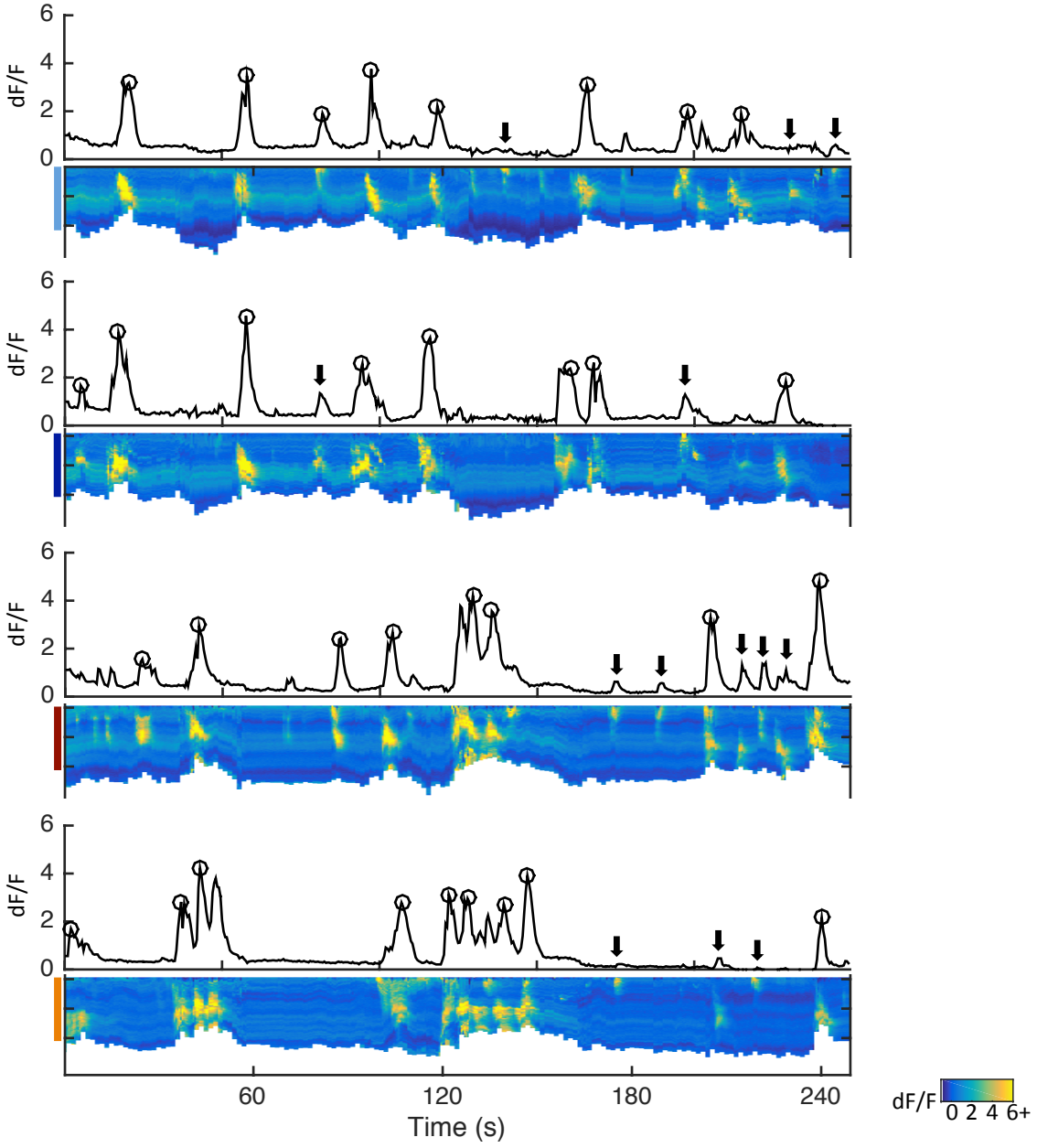

Supp Fig 3

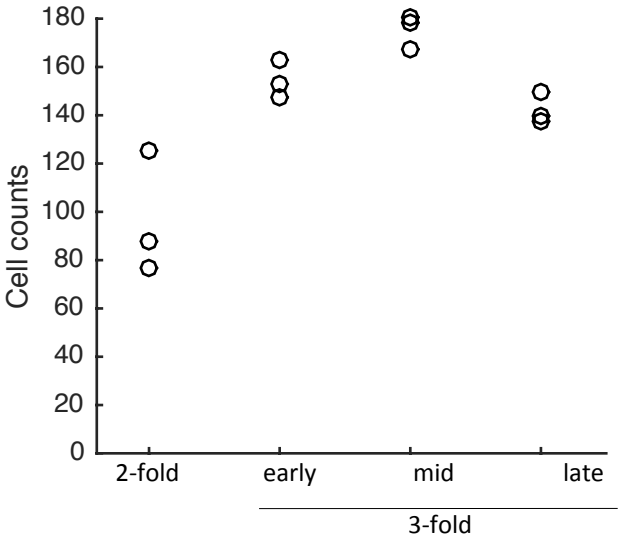
Cell counts
180
160
140
120
100
80
60
40
20
0
2-fold
early
mid
late
3-fold

Supp Fig 4

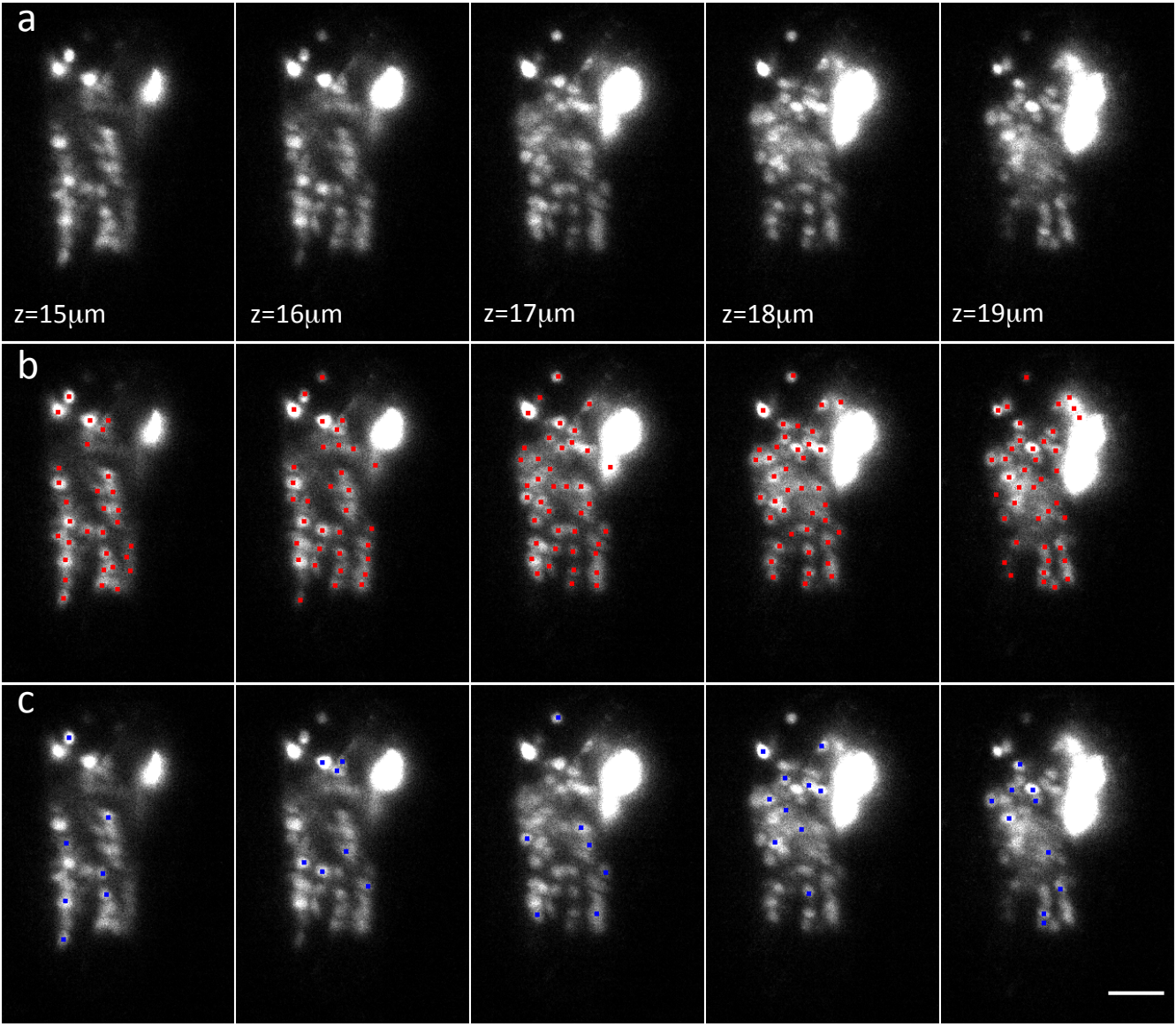

Supp Fig 5

a

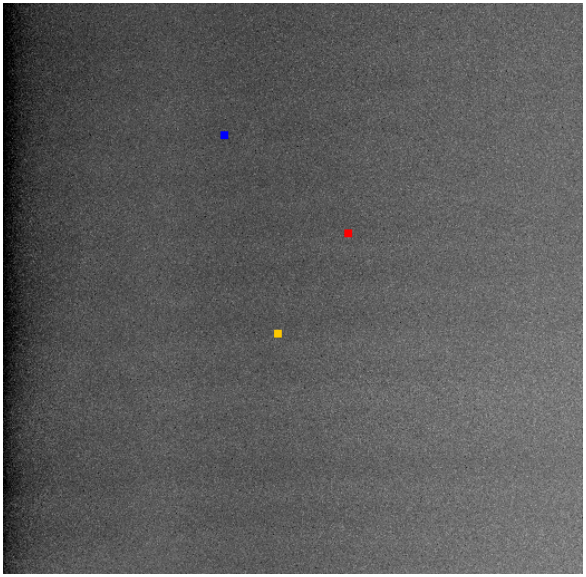

b

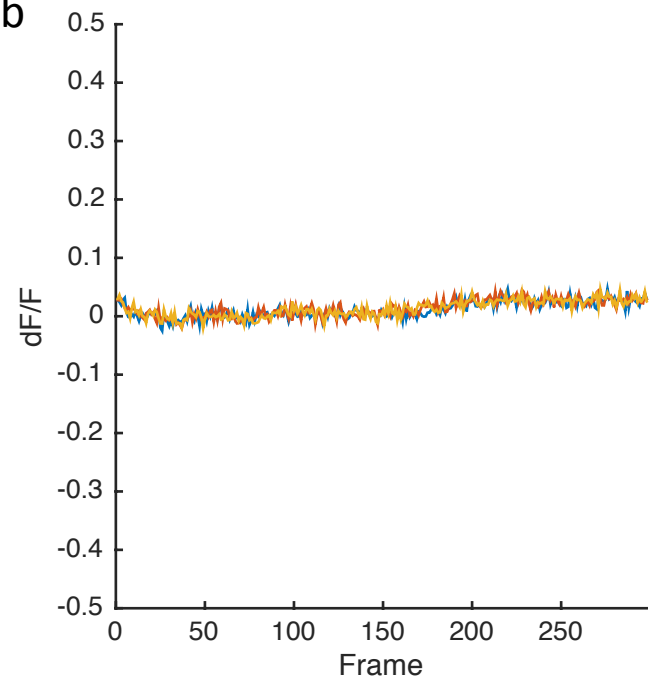

Supp Fig 6

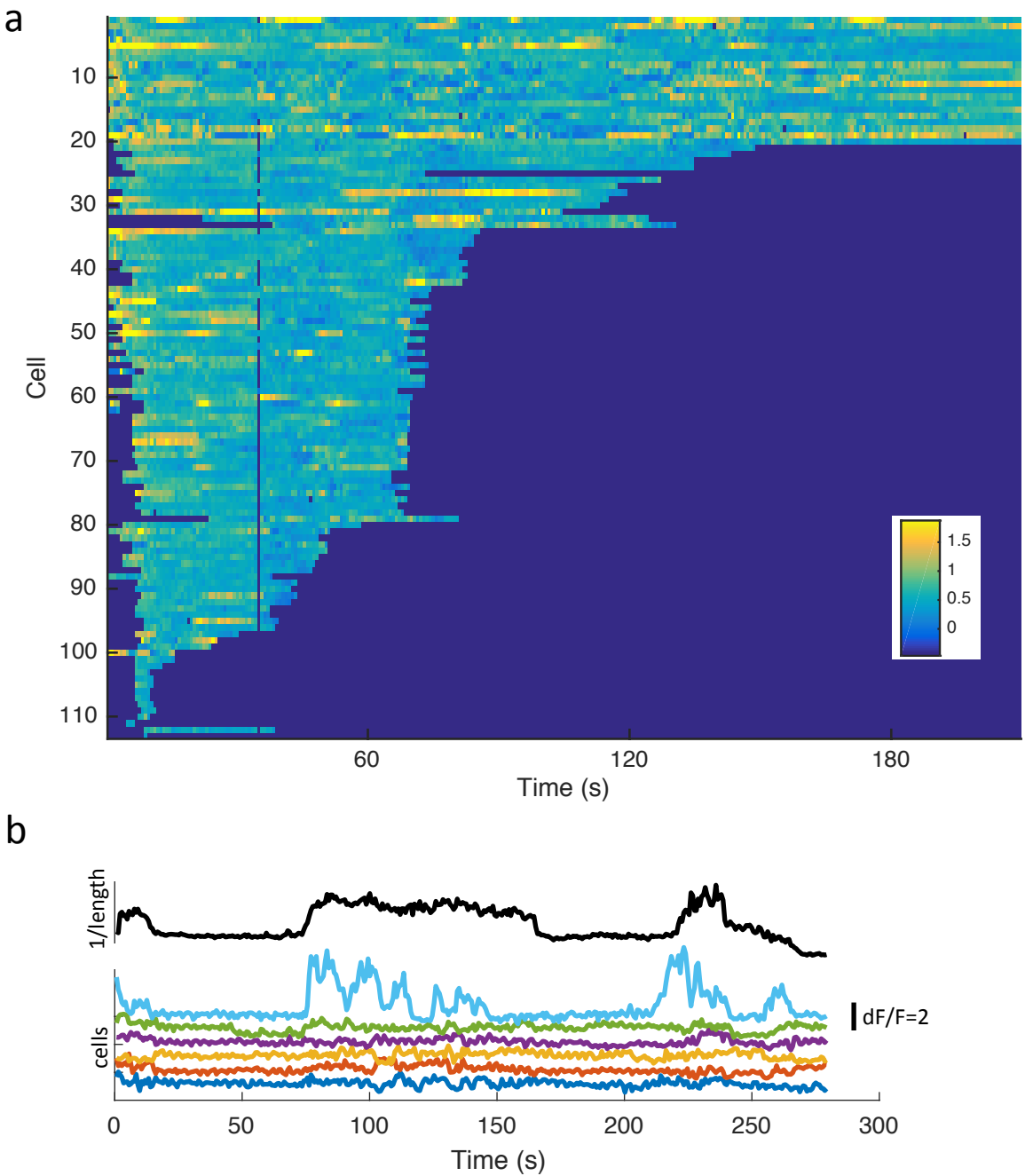
a
Cell
10
20
30
40
50
60
70
80
90
100
110
60
120
180
Time (s)
1.5
1
0.5
0
b
1/length
cells
dF/F=2
0
50
100
150
200
250
300
Time (s)

Supp Fig 7